

Supplementary Information

Enhanced selectivity, cellular uptake, and *in vitro* activity of an intrinsically fluorescent copper-tirapazamine nanocomplex for hypoxia targeted therapy in prostate cancer

Vera L. Silva¹, Abdessamad Kaassis^{1,2}, Ashkan Dehsorkhi¹, Cédrik-Roland Koffi², Maja Severic², Moustafa Abdelhamid¹, Duuamene Nyimanu^{1,3}, Christopher J. Morris¹, and Wafa' T. Al-Jamal^{1,2*}

¹*School of Pharmacy - University of East Anglia, Norwich Research Park, Norwich, NR4 7TJ, United Kingdom*

²*School of Pharmacy – Queen's University Belfast, Belfast, BT9 7BL, United Kingdom.*

³*Experimental Medicine and Immunotherapeutics, University of Cambridge, Centre for Clinical Investigation, Addenbrooke's Hospital, Cambridge, CB2 0QQ, United Kingdom.*

**Corresponding author*

Dr Wafa' T. Al-Jamal

School of Pharmacy

Queen's University Belfast

Belfast, BT9 7BL, United Kingdom

E-mail: w.al-jamal@qub.ac.uk

Table of Contents

1. Experimental section
2. Results
3. Figures and tables

Figure S1: ATR-FTIR spectra of TPZ and Cu(TPZ)₂.

Figure S2: Fourier Transform Mass Spectrometry (FTMS) spectrum of: A) protonated TPZ, and MALDI-MS (Matrix-assisted Laser Desorption/Ionization Spectrum Mass Spectrometry) of B) Cu(TPZ)₂ complex

Figure S3: Partition coefficient determination by shake-flask method

Figure S4: XRD spectrum of the Cu(TPZ)₂ complex in the powder form.

Figure S5: UV/Vis characterization and stability of TPZ and Cu(TPZ)₂ complex.

Figure S6: Stability of Cu(TPZ)₂ in 50% serum.

Figure S7: Fluorescence characterization and stability of TPZ and Cu(TPZ)₂ complex.

Figure S8: Hypoxia validation in C4-2B and LNCap prostate cancer cells.

Figure S9: Nuclear co-localization of Cu(TPZ)₂ uptake in C4-2B cells after 1 h incubation

Figure S10: Cellular uptake of TPZ in C4-2B prostate cancer cells.

Figure S11: IR spectra of cell lysate samples incubated with TPZ (100 μM) for different duration (1,4,8,24 h).

Figure S12: IR spectra of cell lysate samples incubated with Cu(TPZ)₂ (50 μM) for different duration (1,4,8,24 h).

Figure S13. Analysis of cell viability in C4-2B prostate cancer cells incubated with TPZ and Cu(TPZ)₂ under normoxia and 1% hypoxia.

Figure S14. Analysis of cell viability in LNCap prostate cancer cells incubated with TPZ and Cu(TPZ)₂ under normoxia and 1% hypoxia.

Table S1. IC₅₀ values and hypoxia cytotoxicity ratio (HCR) in two prostate cancer cell lines, following continuous drug exposure under aerobic or different hypoxic conditions

Figure S15. C4-2B prostate cancer spheroids characterization.

Figure S16. Analysis of hypoxia in C4-2B prostate cancer spheroids.

Figure S17. Phase-contrast microscope images representative of C4-2B spheroids (day 5 of culture).

Figure S18. Cell cycle analysis of C4-2B spheroids (day 5), after 72 h post-treatment with TPZ and Cu(TPZ)₂.

Table S2. IC₅₀ values of TPZ and Cu(TPZ)₂, after continuous drug exposure in C4-2B spheroids treated on day 5 of culture

1. Experimental section

Tirapazamine stock solutions

For characterization purposes, tirapazamine was dissolved in either DMSO (56 mM) or ethanol (2.8 mM) and stored in darkness at -20°C. Standard solutions in PBS (pH 7.4), HBS (20 mM HEPES, 150 mM NaCl, pH 7.4) and water, were prepared on a daily basis for subsequent studies. For biological studies, tirapazamine was dissolved in NaCl 0.9% (4.5 mM).

TPZ and Cu(TPZ)₂ characterization

Elemental analysis

CHN analysis was performed for Cu(TPZ)₂ in order to validate the complexation and test the purity of the compound. Briefly, 5 samples containing an empty tin foil capsule and 7 known sulphanilamide (Sigma, UK) standards (weight ranging from 0.2 mg up to 2.0 mg) were carefully weighed by a 4 d.p. Sartorius scale. All samples were prepared in tin foil capsules that were subsequently closed into a ball formation using tweezers. These samples were used for instrument calibration and generation of a standard curve for further quantitative analysis. Furthermore, a known sample of Cu(TPZ)₂, within the

range of the standard curve was also weighed out and prepared in triplicate. Analysis were performed using a Carlo Erba EA 1108 Elemental Analyser.

Fourier-transform infrared spectroscopy (FTIR) measurements

Solid samples of TPZ and Cu(TPZ)₂ were studied using a Perkin-Elmer BX ATR-FTIR spectrometer. The spectra were recorded in a range between 600 and 4000 cm⁻¹ after 32 scans by correcting the background. Only diagnostic and/or intense peaks were reported.

Mass spectrometry

Samples of TPZ and Cu(TPZ)₂ were mixed at 1:1 volume ratio, with a universal matrix [mixture of 2,5-dihydroxybenzoic acid (DHB) and α -cyano-4-hydrocinnamic acid (CHCA)]. The combined sample and matrix were dropped onto a metal target plate and dried before analysis. Analyses were recorded on a Shimadzu Axima CFR Plus Maldi TOF Mass Spectrometer, with a variable repetition rate 50 Hz N₂ laser with a wavelength of 337 nm. High resolution mass spectrometry was also determined at the EPSRC Mass Spectrometry Unit at the University of Wales, Swansea.

Geometry optimization

The geometry optimization of the Cu(TPZ)₂ was performed using Forcite with the following parameters: Algorithm: Smart, Convergence tolerance (Energy: 2e⁻⁰⁰⁵ kcal/mol, Force: 0.001 kcal/mol/A, Displacement: 1e⁻⁰⁰⁵ A, Maximum number of iterations: 5000.

UV/Vis spectrophotometry

UV/Visible spectroscopic measurements were performed at room temperature, using a Perkin Elmer Lambda 35 (Perkin Elmer, USA) double-beam spectrometer, and a quartz cuvette (10×10 mm). A full absorption spectra scan (190-1100 nm) was performed for an appropriate linear range of concentrations of TPZ (0-280 μ M) and Cu(TPZ)₂ complex (0-50 μ M) in DMSO. After determination of λ_{max} for the main stock solutions, the spectra were further analyzed after dilution in PBS (10 mM and 100 mM, pH 7.4) and HBS (20mM HEPES, 150 mM NaCl, pH 7.4). All scans were performed in triplicate (Scan rates 240 nm/min, slit: 2.0 nm), and the spectra were corrected using the appropriate blanks.

LogP measurements

To determine the partition coefficient, the shake- flask method was adapted ¹. The compounds were first dissolved in DMSO and added to a 1:1 (v/v) of octanol/water. Mixing was then achieved by vortexing at room temperature to establish the partition equilibrium. The solution was then left on a shaker for 2h, to ensure full mixture. Next, the two phases were separated by centrifugation at 3000 xg for 5 min and samples of TPZ and Cu(TPZ)₂ from both phases were determined using a Perkin Elmer Lambda 35 (Perkin Elmer, USA) double-beam spectrometer, and a quartz cuvette (10×10 mm). However, due to insolubility of Cu(TPZ)₂ in octanol, these experiments were not reliable. Alternatively, ChemOffice was used to predict lipophilicity. The logP value of a compound was estimated from the sum of the contribution of each fragment type, and the program accounted for steric, electronic and hydrogen bonding interactions, based on Hansch and Leo ².

Spectrofluorometry

The fluorescence maxima of TPZ and Cu(TPZ)₂ were determined by testing a range of concentrations (up to 60 μ M) in DMSO, but further optimized buffered solutions, such as HBS and PBS. A full fluorescence spectral scan, for both excitation (320 – 530 nm) and emission (540 – 700 nm), was performed by transferring 200 μ L of the samples to 96-flat bottom black well plates (Sterilin[®], Thermo Fisher Scientific, UK). Fluorescence spectral analysis was performed using a CLARIOstar Omega microplate reader (BMG labTechnologies) (filter, bandwidth 10 nm, focal height 8.7 mm and 154 wavelength scan points) and gain adjustment for the maximum fluorescent sample at 25°C. The fluorescence was captured, digitized, and stored on a computer using MARS data analysis software (Version 3.02). The analysis was further performed as endpoint measurements with the appropriate fluorescent filters and triplicate samples. All spectra were corrected using the appropriate blanks.

pH stability study

TPZ and Cu(TPZ)₂ were pre-dissolved in water at pH ranging from 1 up to 12.5. UV/Vis spectrophotometry and spectrofluorometry were carried out as described above. Solutions of Cu(TPZ)₂ were adjusted to a basic pH with NaOH_(aq) and to acidic pH with HCl_(aq).

Complex stability in serum

25 μM of the complex was incubated with 3 mL of FBS: HBS (1:1 v/v). This solution was then placed into a pre-swelled Pur-A-Lyzer™ Maxi Dialysis tube (Fisher Scientific, UK) with 12 kDa molecular weight cutoff. The dialysis tube was incubated in 30 mL release media (HBS containing 1% Tween-80) at 37 ± 0.5 °C, with stirring at 100 rpm, at predetermined time intervals (up to 72 h), triplicate 1 mL samples were taken and replaced with fresh media. The amount of Cu(TPZ)₂ in the samples was then determined by HPLC. Cu(TPZ)₂ samples were prepared in methanol: isopropanol (86:4, %v/v) adjusted to pH 2 with HCL to induce the dissociation of the complex into free TPZ.

HPLC analysis was performed using a Phenomenex® Luna Phenyl-Hexyl column (100 mm x 4.60 mm, 5 μm beads), as it provides unique selectivity for aromatic and moderately polar analytes. The analysis was performed using an Agilent technologies 1200 series HPLC system, with a G1367B automated sample injector (20 μL sample). The mobile phase consisted of 22% methanol in water and was delivered isocratically at a flow-rate of 1.0 ml/min. Absorbance of the column effluent was monitored using a Diode Array Detectors (DAD G4212A/B) set at 270 nm. HPLC analysis was performed as described above and standard curves were generated for both TPZ (Y = 30.4x - 42.06, R²=0.9957) and Cu(TPZ)₂ (Y = 58.33x + 55.15, R²=0.9996). Results were expressed as mean ± SD of cumulative release for triplicate samples of three independent experiments (n=3).

Transmission electron microscopy (TEM)

Imaging was performed with a JEOL, JEM 2010 microscope running a LaB6 (lanthanum hexaboride crystal) emitter at an accelerating voltage of 200 kV. TEM samples were prepared by drop-casting a dilute suspension of the Cu(TPZ)₂ sample (2 mM and 20 μM), dispersed in EtOH to allow solvent evaporation, onto a 200-mesh carbon-coated copper grid (Agar Scientific). The samples were left to dry for 30 s at room temperature, before the measurement. TEM micrographs were taken at different areas of the grids, to ensure the imaging of a large number of particles.

X-ray powder diffraction (XRD)

X-ray diffraction was performed using a Panalytical X'Pert diffractometer operating at 40 kV and 40 mA with Cu Ka radiation (λ = 1.5418 Å). The Cu(TPZ)₂ powder was finely ground and mounted on a sample holder for measurement. Diffracted intensity from the sample holder did not interfere with the Cu(TPZ)₂ characterization. Single-crystal X-ray diffraction measurement was not possible to perform due to the small size of the complex crystals.

Biological studies

Preparation of C4-2B tumor spheroids

C4-2B spheroids were cultured in 96-well flat-bottom plates (Nunc™ Delta Surface plate) (Sigma-Aldrich, UK) using the liquid overlay technique³. Briefly, 100 μL of autoclaved 1% agarose (Sigma, UK) was cast into 96 flat-bottom well plates and used fresh or stored in the fridge for up to 1 week. C4-2B cells were detached using 0.05% trypsin/EDTA and seeded (5x10³ cells/well) in agarose pre-coated 96-well plates. Plates were gently shaken to facilitate the formation of a single spheroid. 3D cultures were maintained in normal culture conditions in a humidified chamber at 37°C and 5% CO₂.

To maintain spheroid culture, the old medium was replenished every two days by removing 100 μL and replacing it with fresh media, taking care not to disturb the spheroids. Spheroid growth was monitored over time and more than 30 spheroids were imaged on a daily basis, using light microscopy (Olympus CKX41 microscope with a 10x objective and an attached Micropublisher 3.3 RTVcamera).

Images were analysed using the open source software imageJ (NIH, Bethesda, MD, USA: <http://imagej.nih.gov/ij>), applying an image of known scale as calibration. In order to determine spheroids diameter and volume, a previously written macro (Macro S1) was used to automate the process⁴. Diameter and all shape parameters were analysed via ImageJ, then saved and analysed in Excel. The Ferret's diameter (r) was used in the estimation of the mean diameter of the spheroids and to determine their average volume (V) overtime, as follows:

$$V = \frac{4}{3}\pi r^3$$

Moreover, the parameter "circularity" was used to determine the spheroid proximity to a circle (determining their regularity), while the "Solidity" function indicates the roughness of the spheroidal surface. The final results were a good indicator of spheroid uniformity and experimental size reproducibility to ensure less variability during drug treatment studies.

Hypoxia validation in C4-2B spheroid models

Hypoxia was validated using the CYTO-ID[®] Hypoxia/Oxidative Stress Detection kit (Enzo Life Sciences, UK) and images were processed and analysed using ImageJ (NIH, Bethesda, MD, USA: <http://imagej.nih.gov/ij>). Briefly, cells were harvested by trypsinisation and seeded at 5×10^3 cells/well into agarose pre-coated 96 well plates (Triplered, UK). The cells were allowed to grow and were monitored up to 8 days of culture, for hypoxia assessment. 100 μ L of the supernatant was then removed slowly and the spheroids were washed three times with cold PBS, by gently removing and replenishing 100 μ L of the supernatant. The spheroids were then incubated with the hypoxia red probe (500 nM) and unstained cells were used as a negative control. Incubation was performed in normal conditions for 4 h at 37°C. After 4 h, the suspension was removed and the wells were washed three times with cold PBS, as described above. Spheroids at different days of culture were analysed immediately using an inverted Zeiss Axiovert 200M equipped with epifluorescence and a Zeiss ApoTome (Carl Zeiss, UK), Texas Red (596/670 nm) filter, to create optical sections free of scattered light. For each spheroid, a z-stack with 10 μ m intervals was generated. Images were acquired with a 10x/0.45 air objective and Axiovision 4.1.8 software. For each endpoint, three spheroids from two independent experiments ($n=2$) were analysed.

2. Results

Synthesis, chemical and structural characterization of Cu(TPZ)₂

FTIR and MS analysis: TPZ showed ligand bands corresponding to ν_{as} (NH₂)(3409 cm⁻¹) and ν_s (NH₂)(3258 cm⁻¹) that upon coordination were significantly displaced (3360, 3311 cm⁻¹), resulting from deprotonation and formation of a secondary amine upon complexation^{1,5}. Furthermore, the strong vibrational frequency of the N-O stretch for TPZ (1345 cm⁻¹) turned to a weak one upon complexation, indicating the coordination of only one of the N→O groups per ligand molecule, with decreasing π character of the N-oxide bond⁵⁻⁶. Complexation was also confirmed using MS analysis. For TPZ, the molecular ion species [L-Na]⁺ (m/z 201.0382) can be observed as the base peak (**Figure. S2A**). The complex presented one major ion species corresponding to one copper coordinated to two deprotonated TPZ ligand molecules [(Cu-L)-H]⁺ (m/z 418.0202) (**Figure. S2B**), thus confirming the 2:1 stoichiometry of the cupric complex. These results validated previous tentative assignment of TPZ-Cu(II) binding sites at the 3NH₂ and 4NO positions⁷ and the proposed Cu(TPZ)₂ structure (**Figure. 1A**). Derivatives of quinoxalines, such as TPZ, and their complexes have been shown to be stabilized by both electrostatic and covalent interactions of the type Cu⋯N and Cu⋯ π , besides intermolecular hydrogen bonding. These interactions conveyed their essential role in many biological activities⁸.

Log P: Given the difficulty encountered in measuring the logP value for Cu(TPZ)₂ due to its insolubility in octanol (**Figure. S3**), ChemOffice (a user-friendly software) was used to predict this value, using the

fragmental method based on Hansch and Leo⁹. Previous reports have validated that using such *in silico* screening methods can provide a reliable preliminary logP indicator and the fragment method has indeed generated the lowest error and better correlation with experimental data¹⁰⁻¹¹. After running the simulation, a logP of 2.88 was obtained for the cupric-complex, evidencing its increased lipophilic nature. This result is in line with previous reports¹²⁻¹³, which have shown a good correlation between the enhanced lipophilic nature of a cupric complex, after coordination of copper (II) to the N3 position of the ligand.

Solubility and stability of Cu(TPZ)₂ in different media

Facilitating their biological application, we further evaluated the solubility and stability of TPZ and its copper complex in different media, using UV-Vis spectrophotometry. Our results showed that TPZ was soluble in polar solvents, such as water, methanol and ethanol. On the other hand, the developed Cu(TPZ)₂ complex was soluble in DMSO, and partially soluble in polar solvents, such as methanol and aqueous buffers.

Furthermore, the optical properties of the two compounds in different aqueous media were studied (**Figure. S5**). TPZ showed an intense absorption peak at 462 nm in a range of aqueous buffers (**Figure. S5A**), indicating good stability of TPZ in different buffers and pH (**Figure. S5B**), except at pH 12.5, as previously shown¹⁴. Contrary to TPZ spectrum, the developed Cu(TPZ)₂ showed two shoulder bands at 555 and 595 nm in aqueous buffers (**Figure. S5C**), typical from d-d transitions, which could suggest a distorted square planar structure of the complex which requires further investigations. This low-resolution bandwidth in the electronic spectra can be attributed to Jahn-teller distortions, which are common in Cu(II) complexes and contribute to their high stability in solution^{1,5}.

3. Supporting Figures

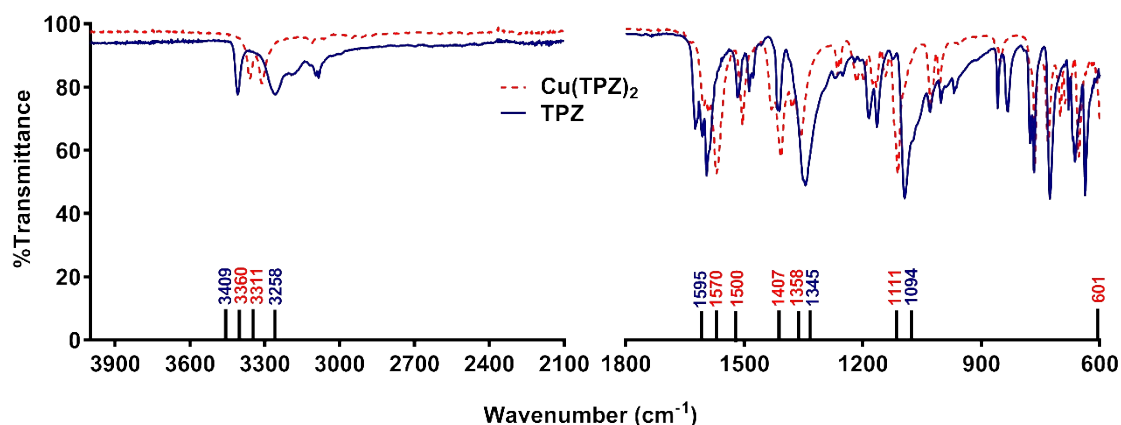


Figure S1. ATR-FTIR spectra of TPZ and Cu(TPZ)₂. FTIR spectra were obtained in the range between 600 and 4000 cm⁻¹ and only diagnostic and/or intense peaks are highlighted. TPZ showed ligand bands corresponding to $\nu_{as}(\text{NH}_2)$ (3409 cm⁻¹) and $\nu_s(\text{NH}_2)$ (3258 cm⁻¹) that upon coordination were significantly displaced (3360, 3311 cm⁻¹), resulting from deprotonation and formation of a secondary amine upon complexation to the copper ion. The strong vibrational frequency of the N-O stretch for TPZ (1345 cm⁻¹) turned to weak upon complexation, indicating the coordination of only one of the N → O groups per ligand molecule. Bands at 1500 cm⁻¹ and 1570 cm⁻¹ derived from $\nu\text{N}=\text{N}$ and $\nu\text{C}=\text{N}\rightarrow\text{O}$, further confirm the involvement of the N-oxide group in complexation. Although poorly resolved, the Cu-NO bending peak can be observed at 601 cm⁻¹.

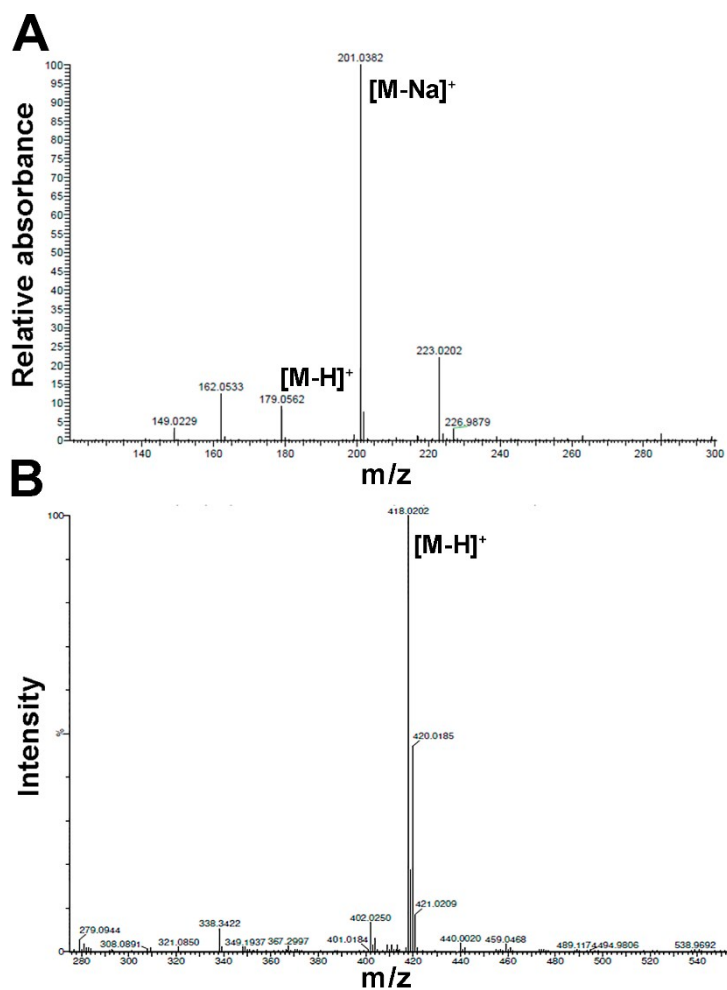


Figure S2. Fourier Transform Mass Spectrometry (FTMS) spectra. A) protonated TPZ, and MALDI-MS (Matrix-assisted Laser Desorption/Ionization Spectrum Mass Spectrometry) of B) Cu(TPZ)₂ complex. For TPZ, the molecular ion species [L-Na]⁺ (m/z 201.0382) can be observed as the base peak. The complex presented one major ion species [Cu (L- H)]⁺ m/z (418.0202), confirming complexation.

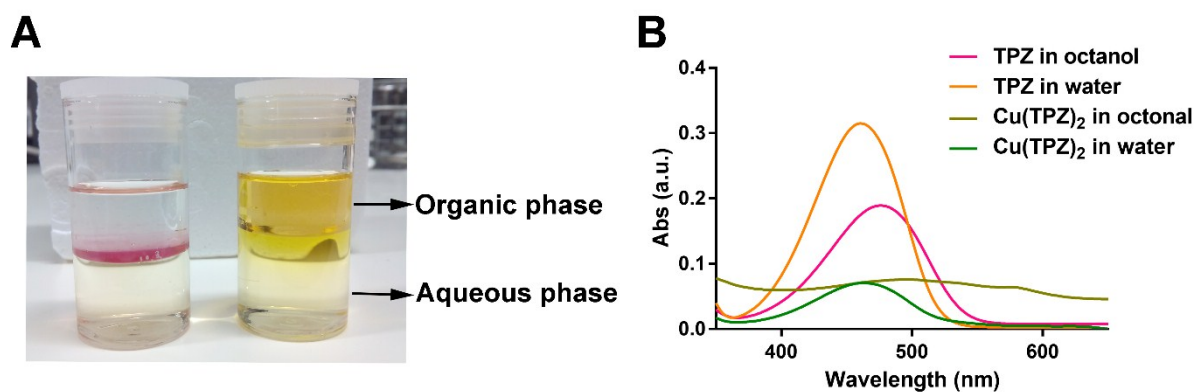
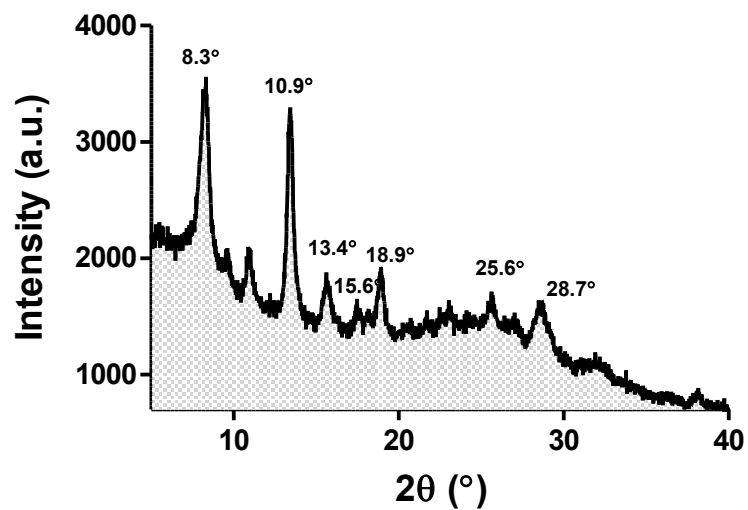


Figure S3. Partition coefficient determination by shake-flask method. A) $\text{Cu}(\text{TPZ})_2$ and TPZ in DMSO were added to 1:1 (v/v) mixture of octanol/water ($20 \mu\text{M}$, final concentration) and the phases allowed to equilibrate. B) UV/Vis spectrum of both compounds after phase separation for quantification. TPZ easily dispersed in both phases, with an evident higher concentration in the aqueous phase. In contrast, $\text{Cu}(\text{TPZ})_2$ settled at the DMSO interface, due to low solubility in octanol. This limited the complex phase separation, retrieval and consequently quantification



Fi

Figure S4: XRD spectrum of the Cu(TPZ)₂ complex in the powder form. Cu(TPZ)₂ powder was characterized using X'Pert diffractometer (Malvern Panalytical, Netherlands) using Cu K α radiation at 40 kV and 40 mA.

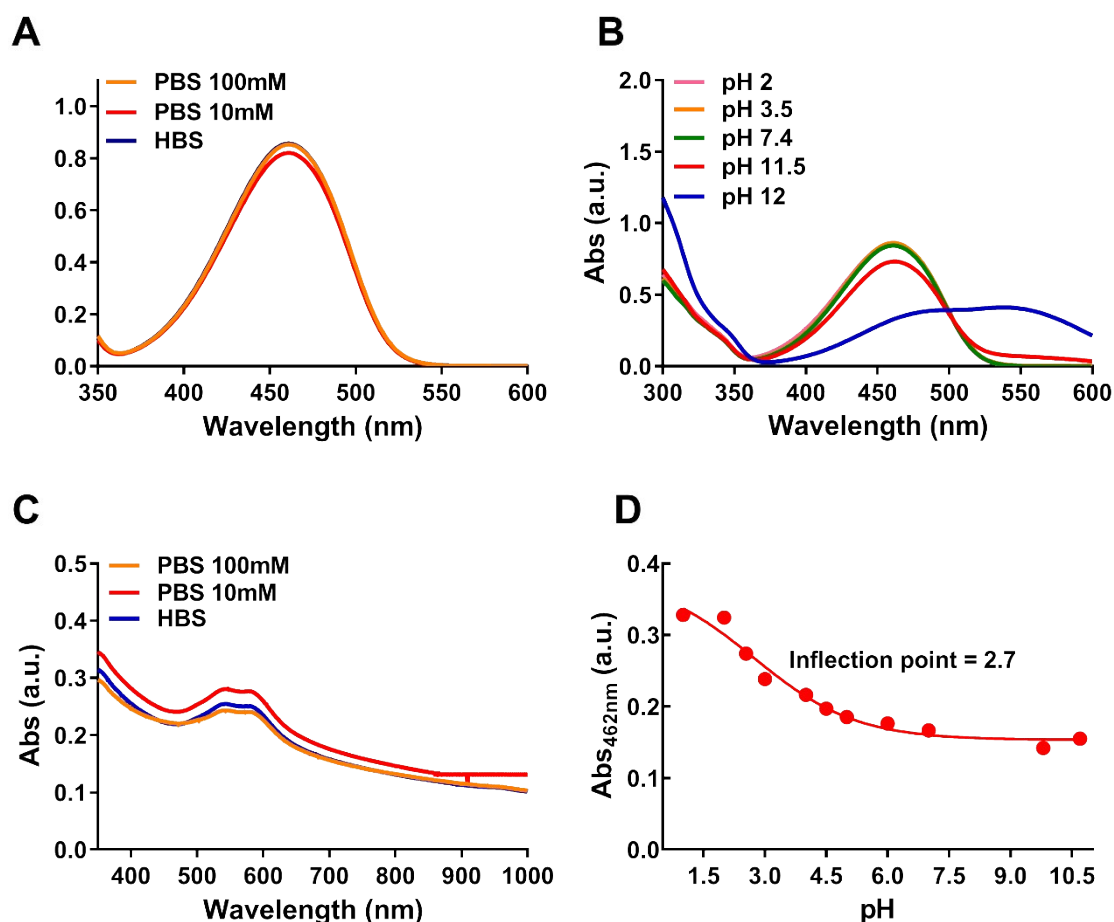


Figure S5. UV/Vis characterization and stability of TPZ and Cu(TPZ)₂ complex. A) UV/Vis spectra of TPZ (168 μ M) in PBS (100 mM, pH 7.4) (red), PBS (10 mM, pH 7.4) (orange) and HBS (20 mM HEPES, 150 mM NaCl, pH 7.4) (blue). B) UV/Vis spectra of TPZ (168 μ M) in water at different pH values (pH 2, 3.8, 7.4, 11.5 and 12.5). C) UV/Vis spectra of Cu(TPZ)₂ (50 μ M) in PBS (100 mM, pH 7.4) (red), PBS (10 mM, pH 7.4) (orange) and HBS (20 mM HEPES, 150 mM NaCl, pH 7.4) (blue) and D) Absorbance of Cu(TPZ)₂ (50 μ M) at 462 nm plotted against pH in water. The calculated inflection point for the fitted sigmoidal curve was 2.7. Appropriate blank solvents were used for baseline corrections.

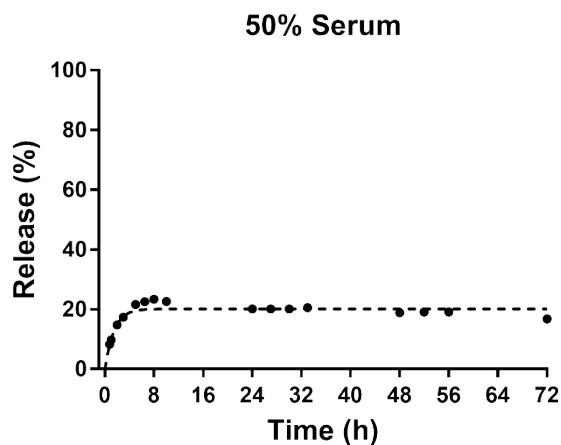


Figure S6. Stability of Cu(TPZ)₂ in 50% serum. 25 μ M of the complex was incubated with 3 mL of FBS:HBS (1:1 v/v). This solution was then placed into a pre-swelled Pur-A-Lyzer™ Maxi Dialysis tube (MWCO12 kDa). The dialysis tube was incubated in 30 mL release media (HBS containing 1% Tween-80) at 37 ± 0.5 °C, with stirring at 100 rpm, at predetermined time intervals (up to 72 h), triplicate 1 mL samples were taken and replaced with fresh media. The amount of Cu(TPZ)₂ in the samples was then determined by HPLC. Results were expressed as mean \pm SD of cumulative release for triplicate samples of three independent experiments (n=3).

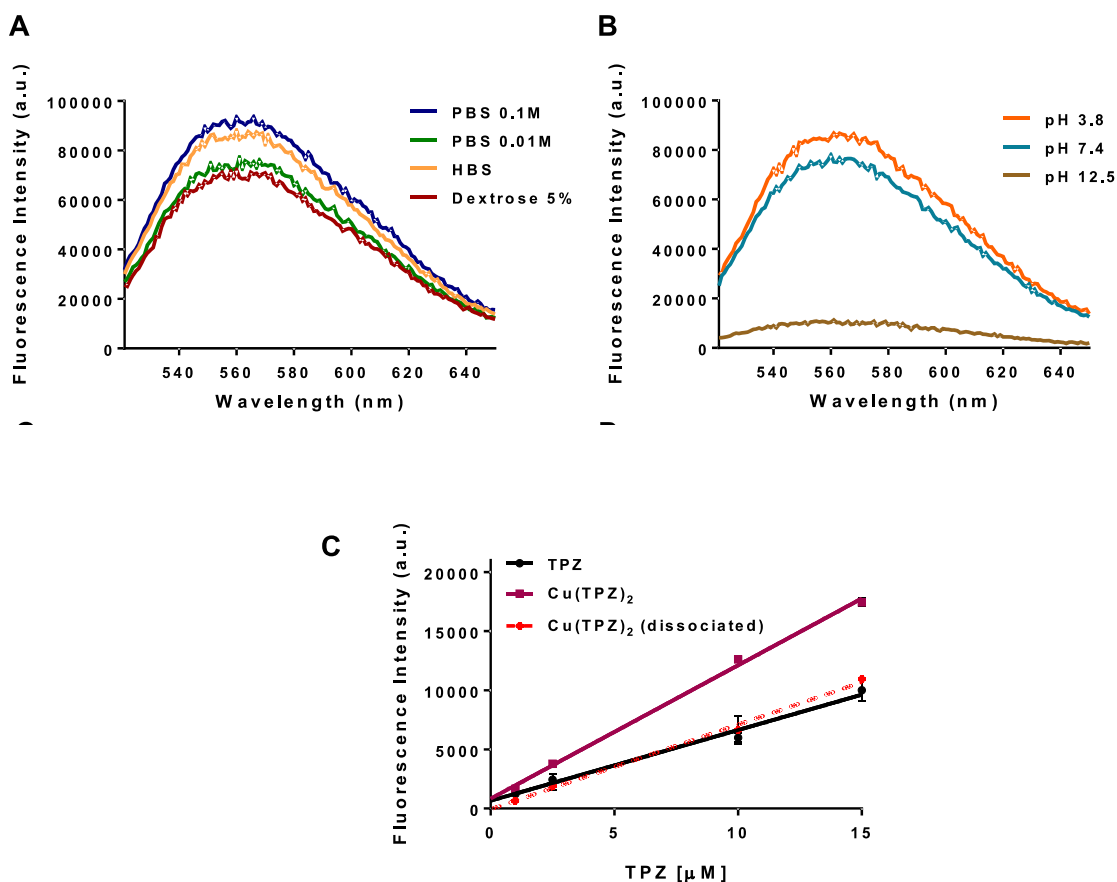


Figure S7. Fluorescence characterization and stability of TPZ and $\text{Cu}(\text{TPZ})_2$ complex. A) Fluorescence spectra of TPZ (168 μM) diluted in PBS (10 mM, pH 7.4) (blue), PBS (100 mM, pH 7.4) (green), HBS (20 mM HEPES, 150 mM NaCl, pH 7.4) (yellow) and dextrose 5% (red); B) fluorescence spectra obtained for TPZ (168 μM) further diluted in water at pH 3.8 (orange), pH 7.4 (blue) and pH 12.5 (brown). The overall fluorescence change was not significant between the different solvents tested. Also, when diluted in different pH values, the spectra remained overall unchanged, aside from pH 12.5, where the emission intensity was decreased; and C) The fluorescence intensity of a wide concentration range of TPZ and $\text{Cu}(\text{TPZ})_2$ dispersed in HBS before and after complex dissociation at pH 2. Appropriate blank solvents were used for baseline corrections of all spectra.

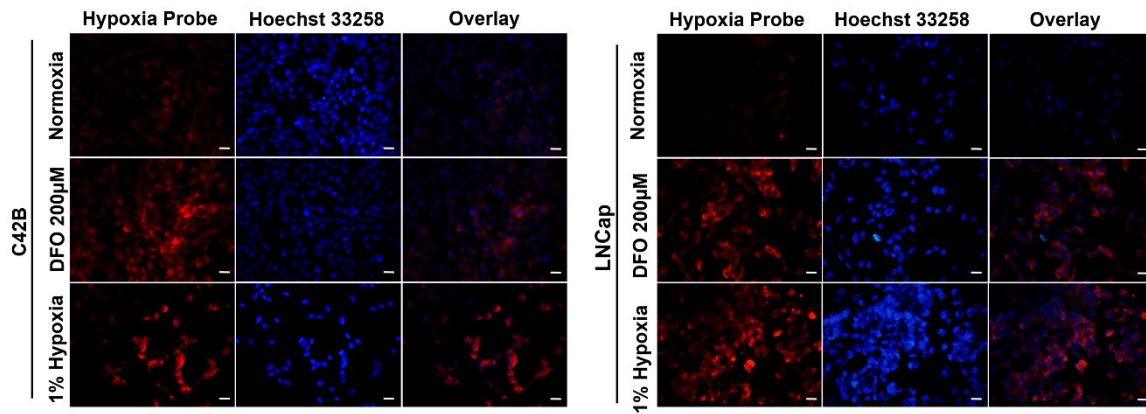


Figure S8. Hypoxia validation in C4-2B and LNCap prostate cancer cells. C4-2B (left) and LNCap (right) cells were incubated under either normoxic (21% O₂, top panels) or hypoxic (1% O₂, bottom panels) conditions. Desferrioxamine (DFO) (200 µM) was used as a chemical inducer of hypoxia (positive control) (middle panels). Cyto-ID[®] Hypoxia detection kit was used to validate hypoxia, following the manufacture's protocol. Fluorescent images are representative of two independent experiments (n=2) and cells were stained with hypoxia probe (red channel) and Hoechst 33258 for nuclei staining (blue channel), scale bar 20 µm.

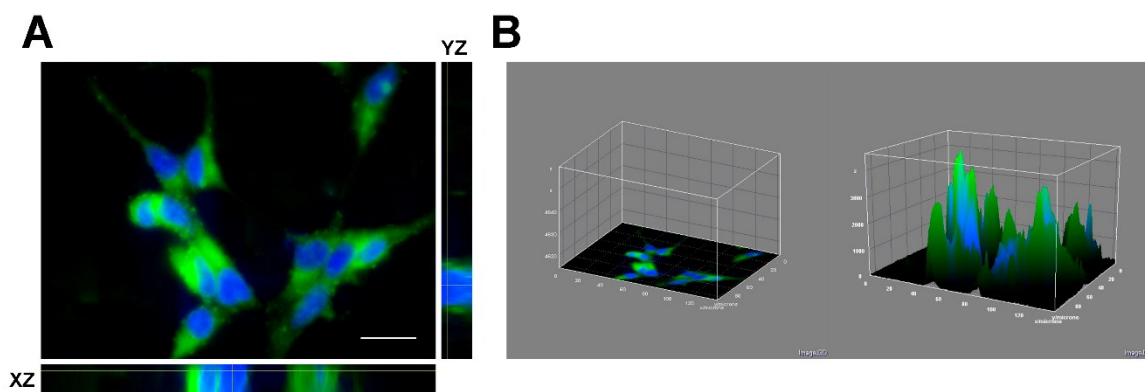


Figure S9. Nuclear co-localization of Cu(TPZ)₂ uptake in C4-2B cells after 1 h incubation. A) Orthogonal projections of the image z-stacks are presented below and to the right of each image, to observe co-localization. B) 3D surface plots of reconstructed 3D images, evidencing intense turquoise signal, due to co-localized fluorescent green signal from the complex and blue signal from the nucleus. Cells were incubated with 100 μ M equivalent TPZ in copper-complexes form. For each image, a Z-stack with 1.75 μ m intervals was generated and images were reconstructed and analysed using imageJ (NIH, Bethesda, MD, USA: <http://imagej.nih.gov/ij>). Images are representative of at least 50 cells of two independent experiments (n=2). Green channel: Cu(TPZ)₂ treated cells; Blue channel: nuclei stained with Hoechst 33258.

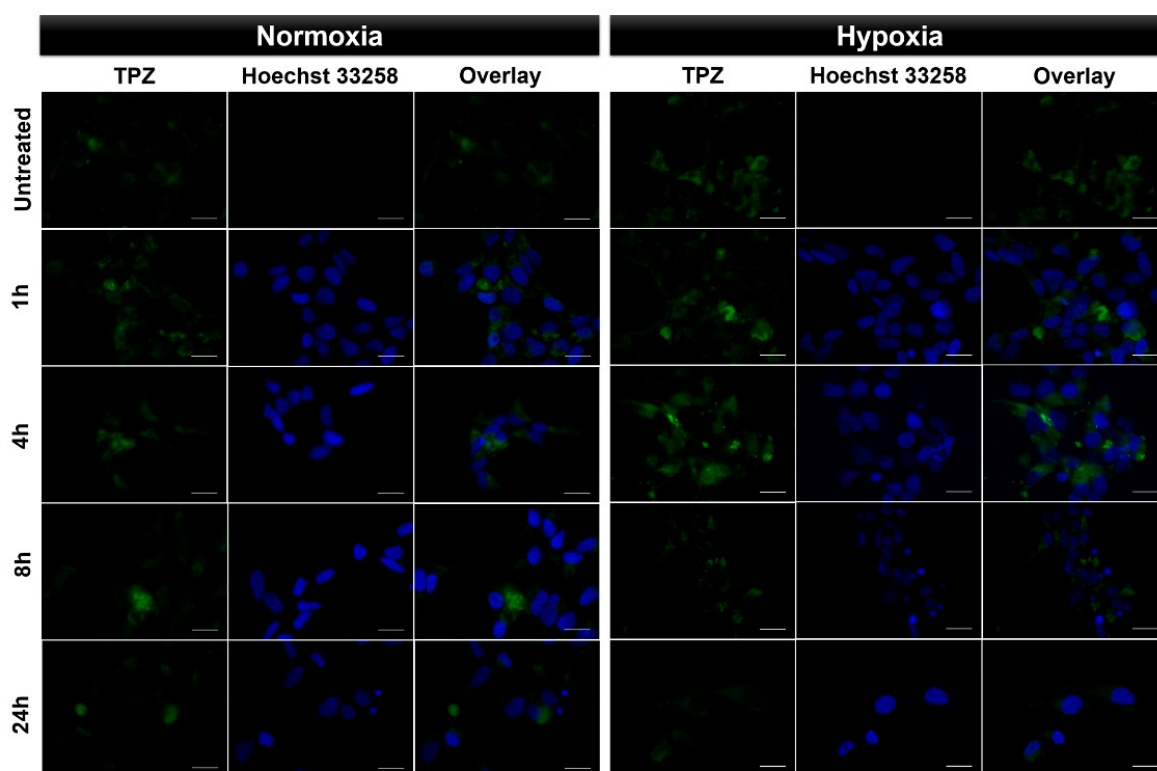


Figure S10. Cellular uptake of TPZ in C4-2B prostate cancer cells. Qualitative uptake of TPZ (100 μ M) was assessed at 1, 4, 8 and 24 h in both normoxia and 1% hypoxia. Images are representative of at least 50 cells of two independent experiments (n=2). Green channel: TPZ treated cells; Blue channel: nuclei stained with Hoechst 33258. Scale bar, 20 μ m.

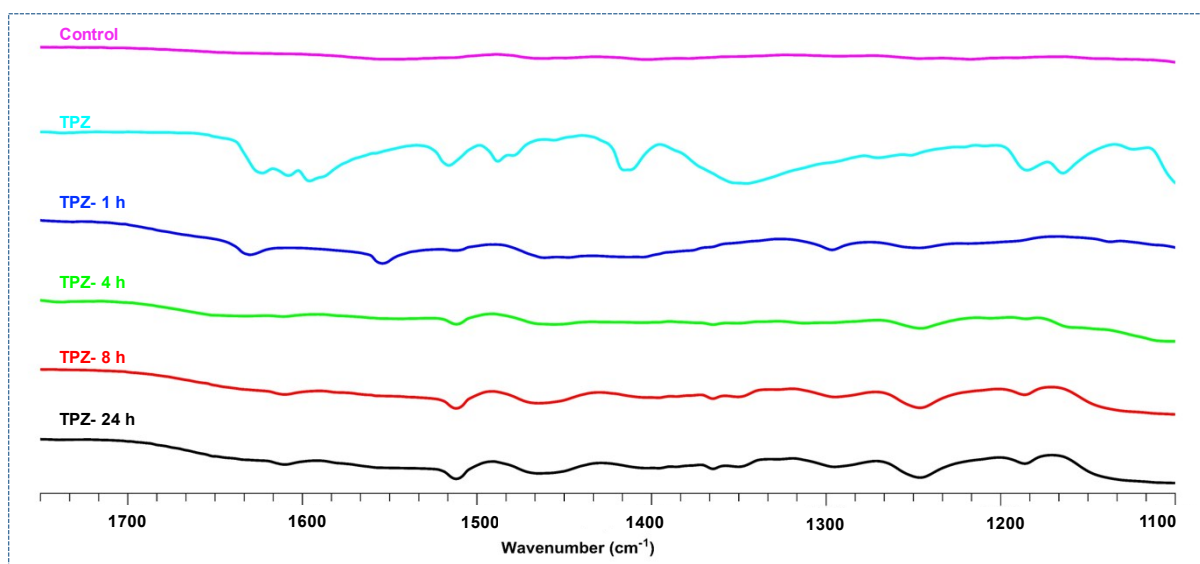
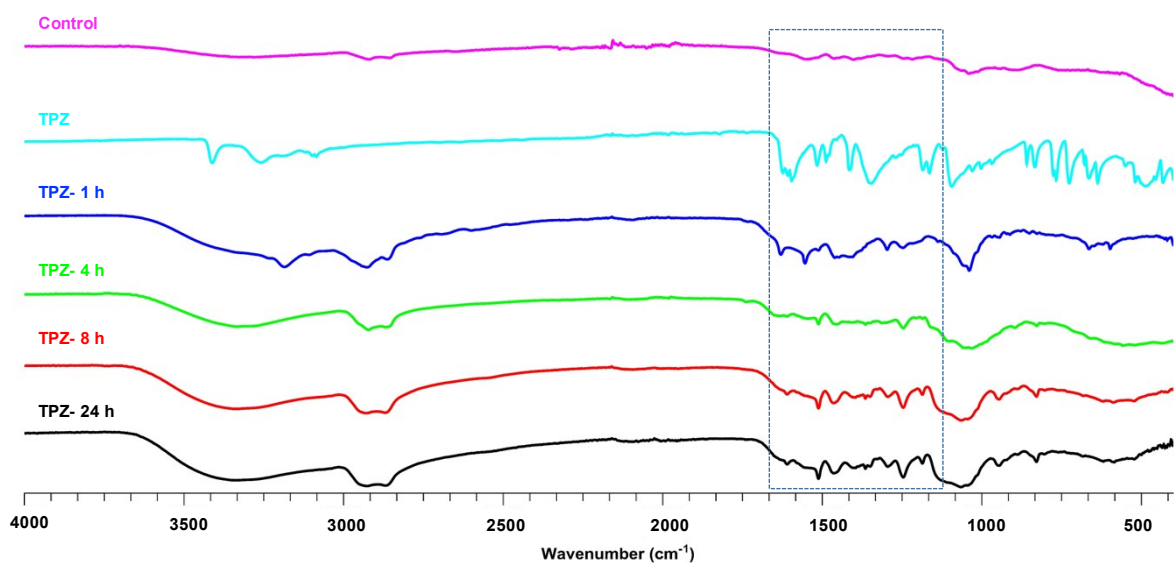


Figure S11. IR spectra of C4-2B cell lysate samples incubated with TPZ (100 μ M) for different duration (1, 4, 8, 24 h). Untreated cells were used as a control. TPZ and was analysed for comparison. Samples were prepared for FTIR analysis as described in the methods section.

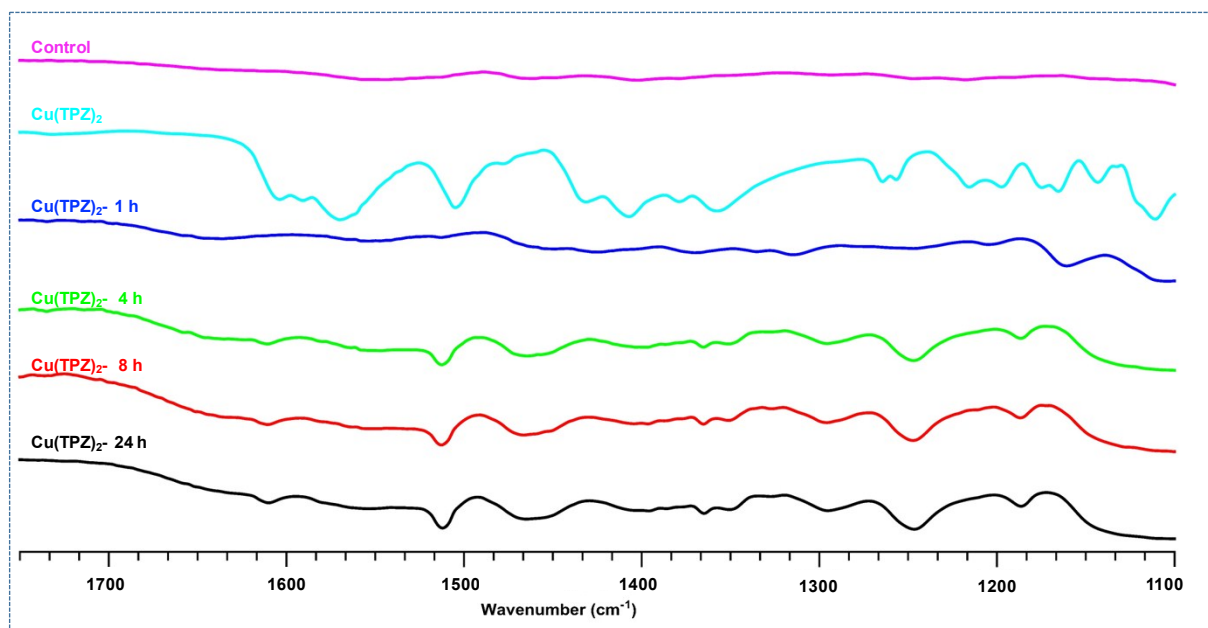
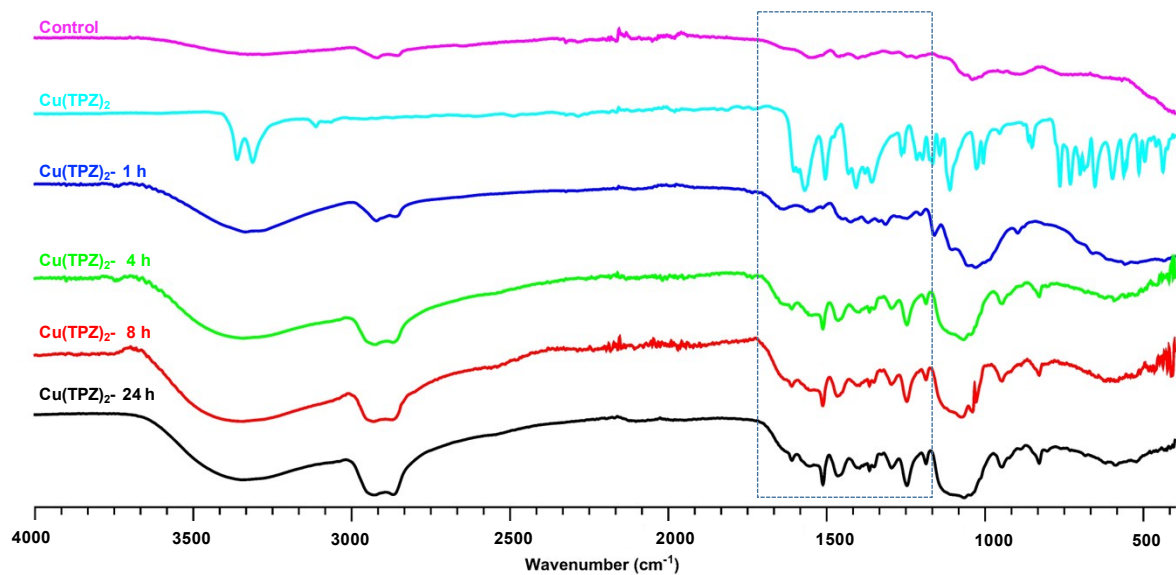


Figure S12. IR spectra of C4-2B cell lysate samples incubated with Cu(TPZ)₂ (50 μM) for different duration (1, 4, 8, 24 h). Untreated cells were used as a control. TPZ and was analysed for comparison. Samples were prepared for FTIR analysis as described in the methods section.

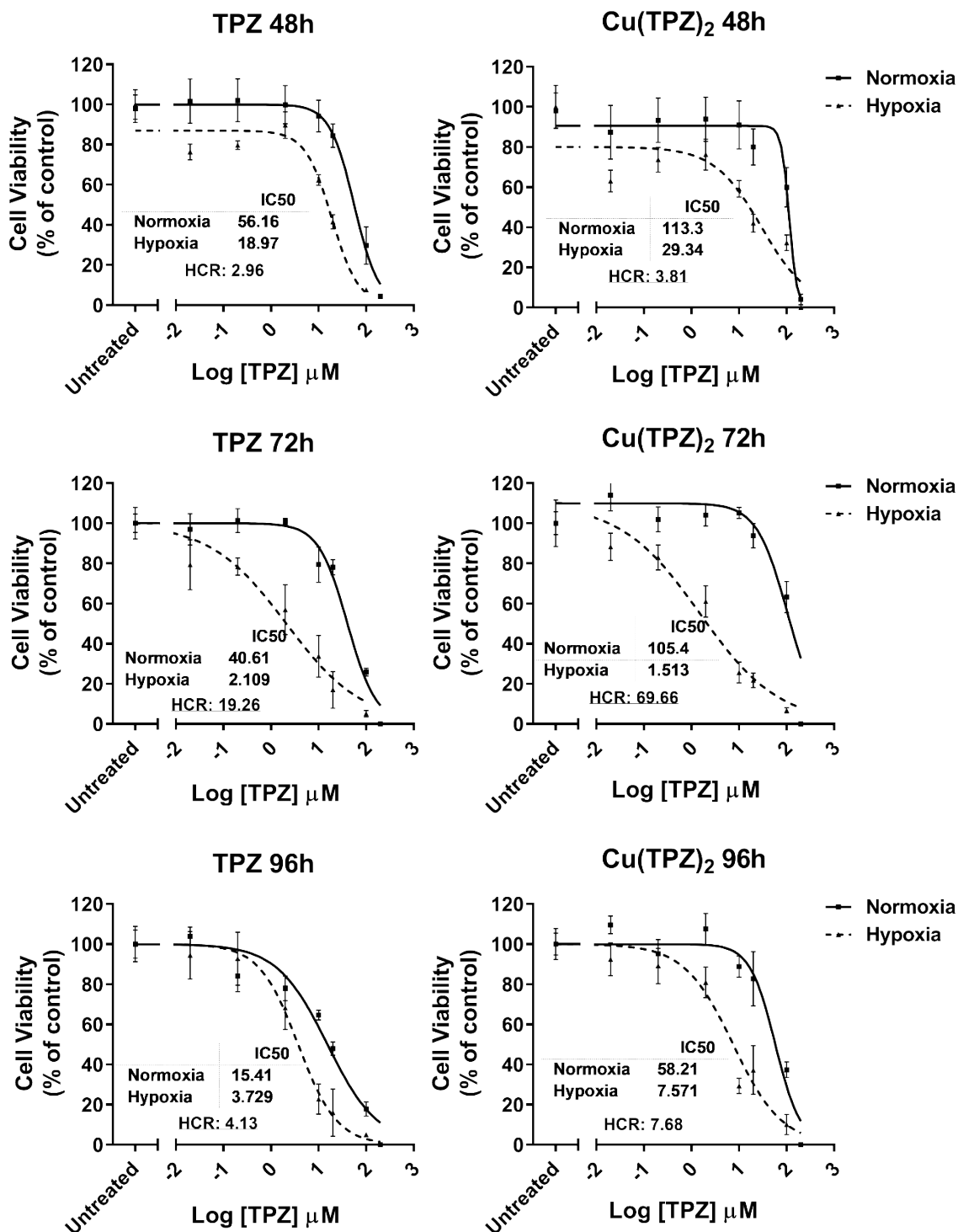


Figure S13. Analysis of cell viability in C4-2B prostate cancer cells incubated with TPZ and Cu(TPZ)₂ under normoxia and 1% hypoxia. C4-2B cells were incubated under both conditions with equivalent doses of TPZ (left panel) and Cu(TPZ)₂ (right panel) for 48, 72, and 96 h. Cell viability was assessed by the resazurin assay, normalized to untreated and results are expressed as mean ± SD for six replicates of three independent experiments (n=3). The IC₅₀ values for inhibition are presented (inset), as determined by nonlinear regression analysis of the data fit to a four-parameter equation (GraphPad Prism version 7.0, GraphPad Software Inc., La Jolla, CA, USA). The hypoxia selectivity is presented as HCR (inset) calculated as the ratio between the IC₅₀ in normoxia and hypoxia.

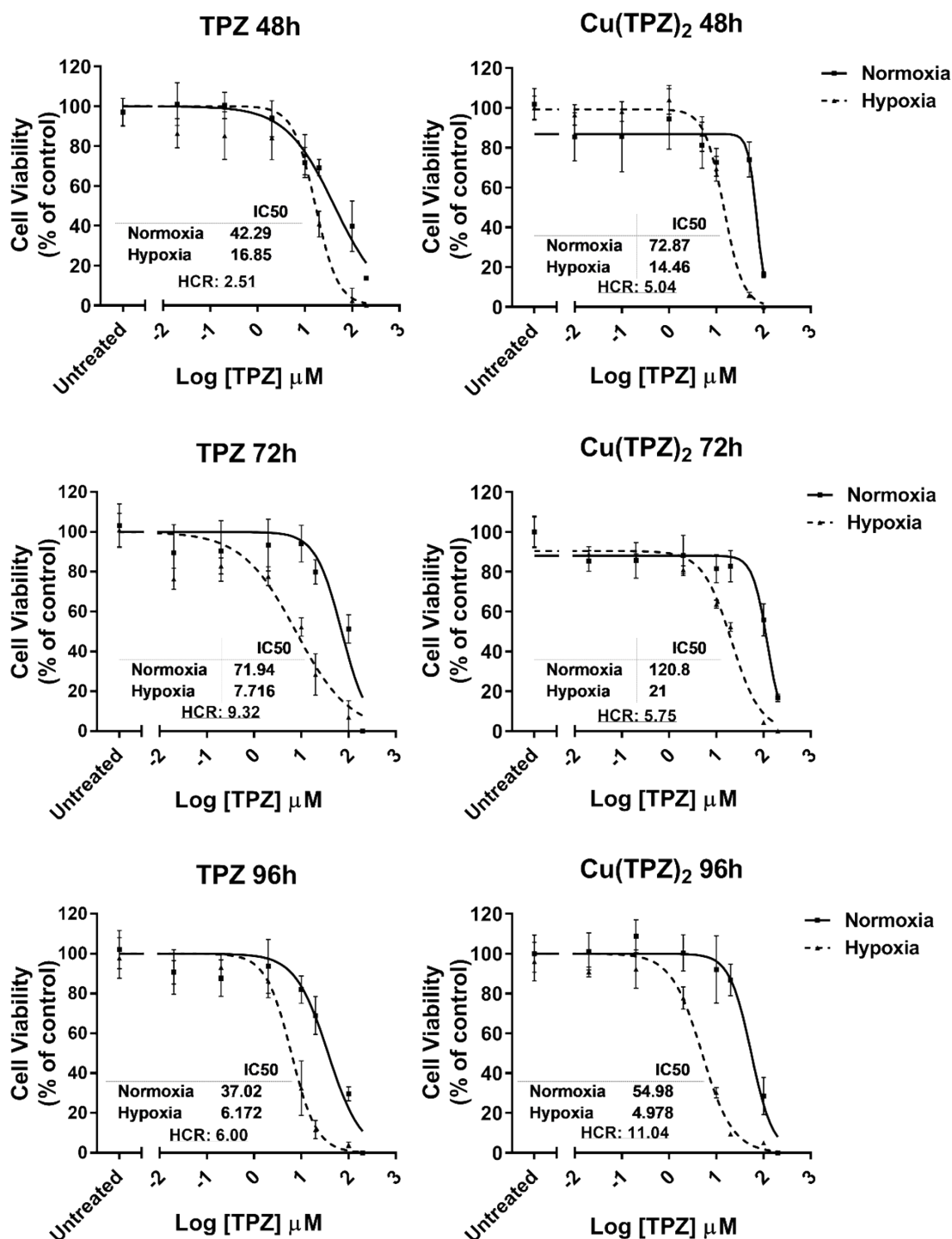


Figure S14. Analysis of cell viability in LNCap prostate cancer cells incubated with TPZ and Cu(TPZ)₂ under normoxia and 1% hypoxia. LNCap cells were incubated under both conditions with equivalent doses of TPZ (left panel) and Cu(TPZ)₂ (right panel) for 48, 72, and 96 h. Cell viability was assessed by the resazurin assay, normalized to untreated and results are expressed as mean ± SD for six replicates of three independent experiments (n=3). The IC₅₀ values for inhibition are presented (inset), as determined by nonlinear regression analysis of the data fit to a four-parameter equation (GraphPad Prism version 7.0, GraphPad Software Inc., La Jolla, CA, USA). The hypoxia selectivity is presented as HCR (inset) calculated as the ratio between the IC₅₀ in normoxia and hypoxia.

Table S1. Summary of IC₅₀ values and hypoxia cytotoxicity ratio (HCR) in C4-2B and LNCap prostate cancer cell lines, following continuous drug exposure under normoxia and 1% hypoxic conditions. Values represent mean ± SD of six replicates of at least two independent experiments (n ≥ 2). IC₅₀ values were determined by nonlinear regression analysis of the data fit to a four-parameter equation (GraphPad Prism version 7).

	TPZ			Cu(TPZ) ₂		
	Normoxia	Hypoxia 1%		Normoxia	Hypoxia 1%	
	IC ₅₀ (μM)	IC ₅₀ (μM)	HCR	IC ₅₀ (μM)	IC ₅₀ (μM)	HCR
C4-2B						
48h	56.16 ± 1.03	31.65 ± 1.02	1.77	114.1 ± 1.01	29.92 ± 1.06	3.82
72h	40.61 ± 1.04	2.831 ± 1.04	14.34	106.4 ± 1.09	1.613 ± 1.04	65.94
96h	15.41 ± 1.14	3.729 ± 1.04	4.13	58.21 ± 1.05	7.571 ± 1.03	7.69
LNCap						
48h	42.29 ± 1.09	16.85 ± 1.02	2.51	72.87 ± 1.78	14.46 ± 1.03	5.04
72h	71.94 ± 1.06	7.72 ± 1.02	9.32	120.8 ± 1.09	21.00 ± 1.04	5.75
96h	37.02 ± 1.05	6.17 ± 1.03	6.00	54.98 ± 1.04	4.98 ± 1.02	11.04

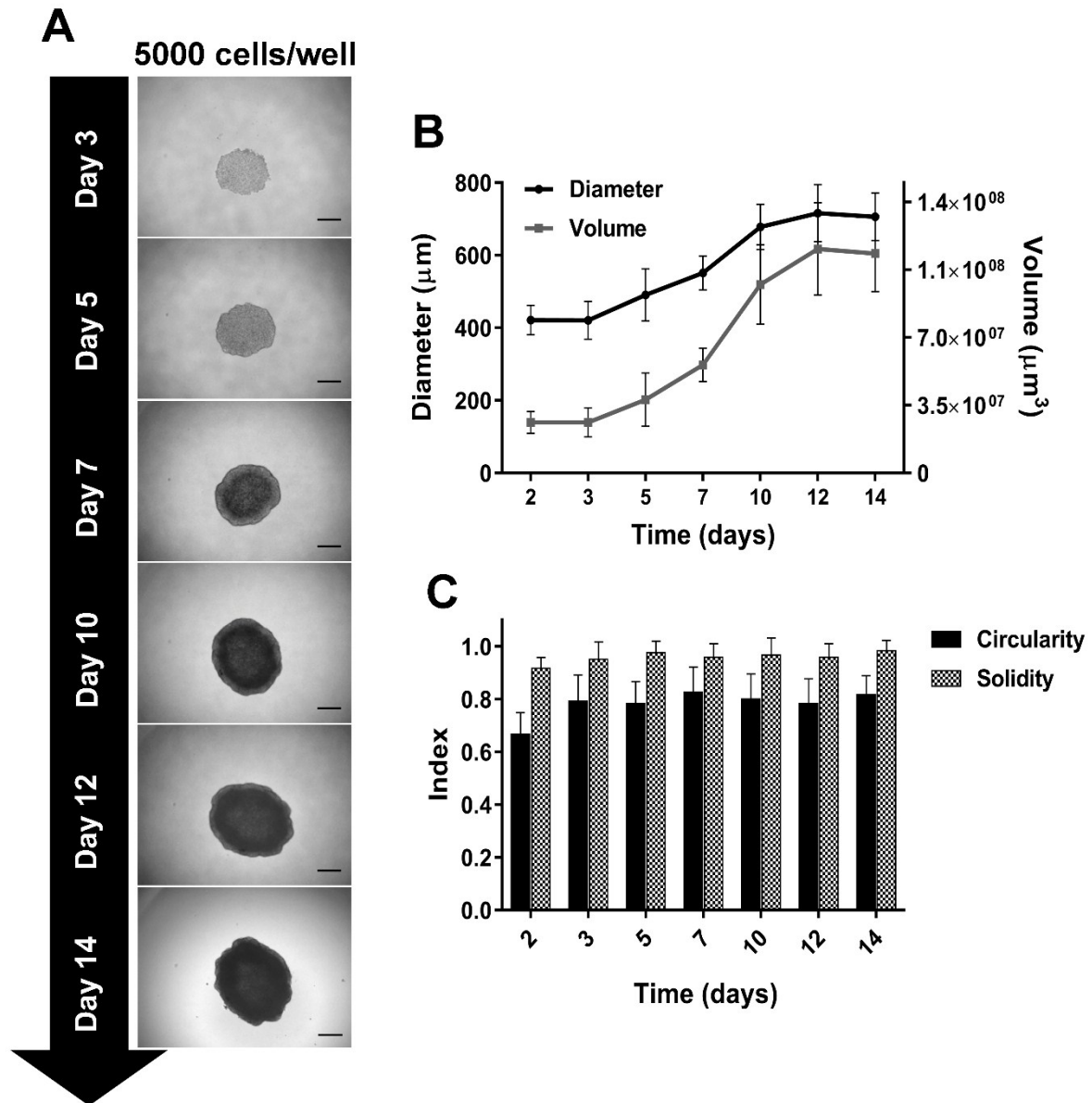


Figure S15. C4-2B prostate cancer spheroids characterization. A) Spheroid growth assay. Representative phase-contrast images of spheroids seeded at an initial density of 5000 cells/well and monitored over a period of 14 days. Spheroids were spontaneously formed and started to fuse from day 2, and were well compacted on day 3. From day 5, the darkest region of the image in bright-field suggests the presence of quiescent/dead cells (necrosis). Scale bars, 200 μm ; B) Spheroid diameter and volume were determined using an automated macro implemented in ImageJ open source software (NIH, Bethesda, MD, USA: <http://imagej.nih.gov/ij>). Spheroid diameters were $421.48 \pm 40.99 \mu\text{m}$ from day 2, achieving values of $706.45 \pm 65.35 \mu\text{m}$ on day 14 and each group was highly uniform ($\text{SD} \leq 10\%$). This was also accompanied by an increased trend in spheroid volume; C) the change circularity and solidity, were also determined using ImageJ, to analyse spheroid uniformity and roughness, confirming circular uniformity and dense morphology of the spheroids. The data represents the mean \pm SD of six replicates of at least two experiments ($n \geq 12$ spheroids), representative of specific growth assays. Further studies using this model guarantee a similar size and characteristics.

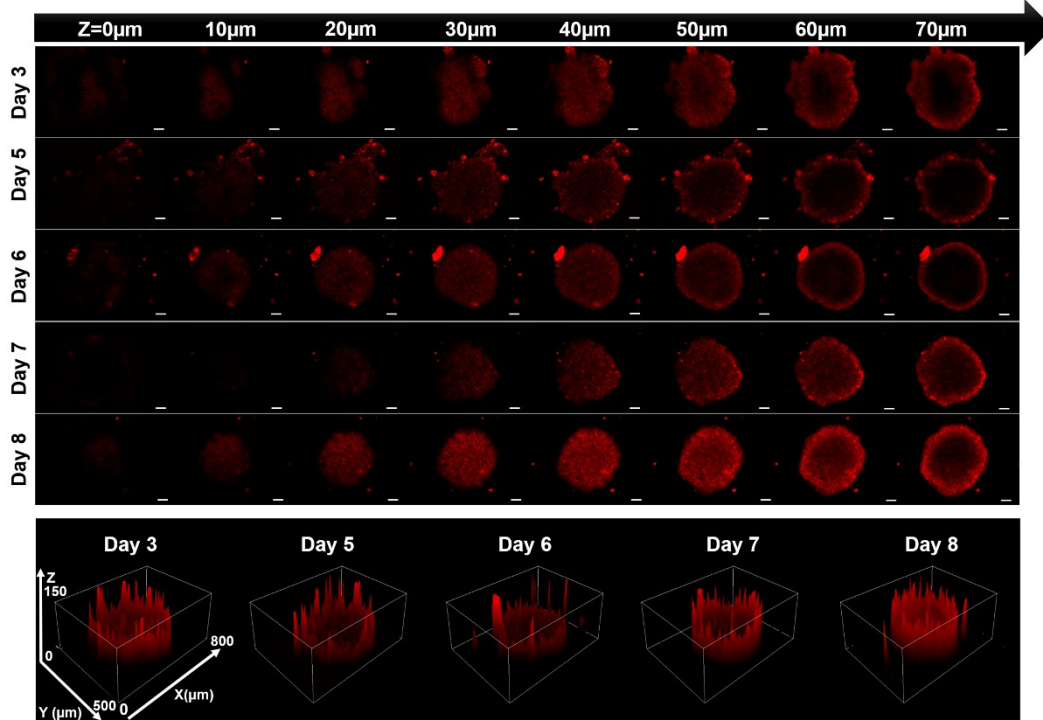


Figure S16. Analysis of hypoxia in C4-2B prostate cancer spheroids. Fluorescent images of 3D C4-2B spheroids incubated with CYTO-ID® Hypoxia Detection probe (500 nM, Enzo Life Sciences, UK) for 4h, taken using an inverted Zeiss Axiovert 200M with Texas Red (596/670 nm) filter and equipped with a Zeiss ApoTome (Carl Zeiss, UK) to create optical sections free of scattered light. For each spheroid, a Z-stack with 10 µm intervals was generated. Scale bar: 100 µm. The bottom panel depicts surface plots of reconstructed 3D images of spheroids, produced in ImageJ (NIH, Bethesda, MD, USA: <http://imagej.nih.gov/ij>). The analysis was performed over 8 days and sections up to 120 µm depth were created, but only sections up to 70 µm were considered, due to the faltered imaging penetration. Hypoxia was visible from day 3 and was seemingly present even at more peripheral areas of the spheroid (< 30 µm), but became more intense and homogeneous at deeper thickness from day 5 (> 40 µm); confirmed by the surface plots generated. These results indicate that the C4-2B spheroids (from day 5), possess heterogeneous expression of hypoxia, which is time-dependent, thus establishing this model as an adequate *in vivo* mimetic of hypoxic tumors.

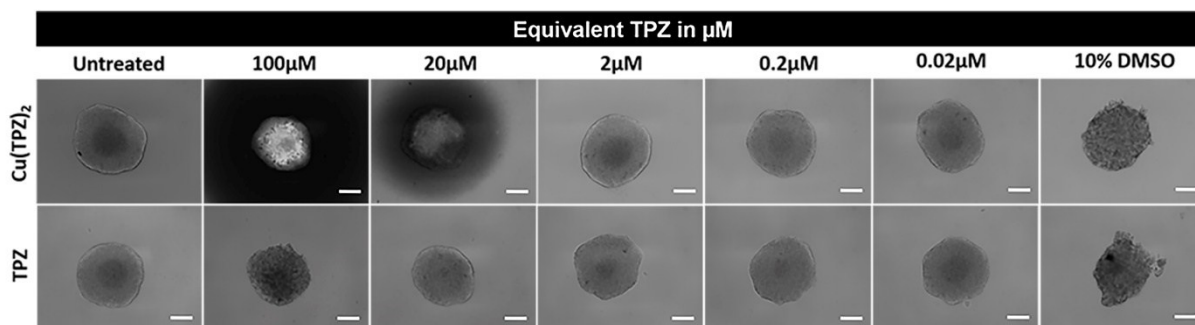


Figure S17. Phase-contrast microscope images representative of C4-2B spheroids (day 5 of culture). Spheroids were exposed to increasing concentrations of Cu(TPZ)_2 and TPZ, after 48 h treatment. Scale bar, 100 μm . Spheroids became more refractive and darker under light microscopy, where cells became looser and recognizable, when exposed to increased doses (100 μM) of TPZ and 10% DMSO. On the other hand, spheroids exposed to high doses of Cu(TPZ)_2 (100 μM equivalent TPZ) appeared smaller in size, compared to control, but seemed to maintain cell compactness. No changes in the spheroids morphology were observed using lower doses of both drugs ($< 2 \mu\text{M}$ equivalent TPZ).

Table S2. IC_{50} values of TPZ and Cu(TPZ)_2 , after continuous drug exposure in C4-2B spheroids treated on day 5 of culture. The IC_{50} values for inhibition were assessed by the resazurin assay after pre-treatment with EDTA (5 mM) for 30 min. Results are expressed as mean \pm SD for six replicates of at least two independent experiments ($n \geq 2$). Statistical analysis: Two-way ANOVA multiple comparison Bonferroni Post-hoc test (**** $p \leq 0.0001$, comparing TPZ vs Cu(TPZ)_2 , GraphPad Prism version 7.0, GraphPad Software Inc., La Jolla, CA, USA).

C4-2B Spheroids (day 5)		
C4-2B	TPZ $\text{IC}_{50} (\mu\text{M}) \pm \text{SD}$	Cu(TPZ)_2 $\text{IC}_{50} (\mu\text{M}) \pm \text{SD}$
48h	35.17 ± 1.17	41.78 ± 5.67
72h	26.21 ± 1.18	25.58 ± 3.78
96h	36.02 ± 1.89	$13.33 \pm 1.43^{****}$

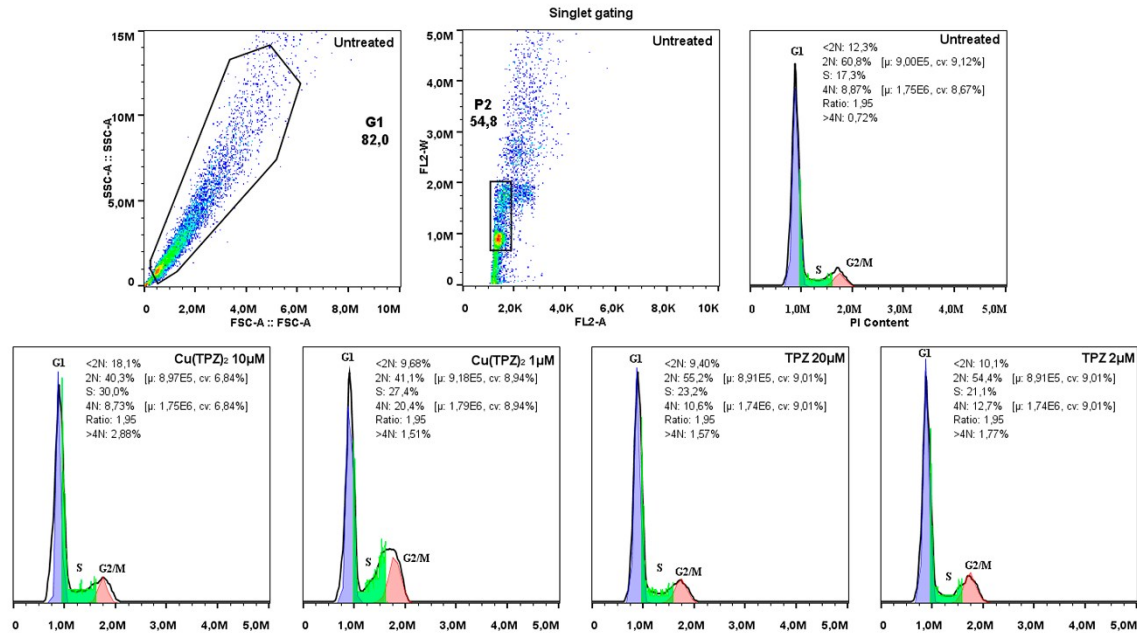


Figure S18. Cell cycle analysis of C4-2B spheroids (day 5), after 72 h post-treatment with TPZ and Cu(TPZ)₂. Spheroids were disassociated, washed, and stained with propidium iodide (PI) for DNA content analysis. Flow cytometry was then used to generate cell cycle profiles. Representative dot plots for cell population and singlet gating are shown, as well as, cell cycle histograms for untreated (upper lane) and treated spheroids (bottom lane). Each flow cytometry plot depicts the percentage of G1 (2n), S and G2/M (4n) fraction population.

References

1. Urquiola, C.; Gambino, D.; Cabrera, M.; Lavaggi, M. L.; Cerecetto, H.; González, M.; de Cerain, A. L.; Monge, A.; Costa-Filho, A. J.; Torre, M. H., New copper-based complexes with quinoxaline N1,N4-dioxide derivatives, potential antitumoral agents. *Journal of inorganic biochemistry* **2008**, *102* (1), 119-126.
2. Hansch, C.; Leo, A.; Hoekman, D. H., *Exploring QSAR.: . Fundamentals and applications in chemistry and biology*. American Chemical Society: 1995.
3. Achilli, T. M.; Meyer, J.; Morgan, J. R., Advances in the formation, use and understanding of multi-cellular spheroids. *Expert opinion on biological therapy* **2012**, *12* (10), 1347-60.
4. Ivanov, D. P.; Parker, T. L.; Walker, D. A.; Alexander, C.; Ashford, M. B.; Gellert, P. R.; Garnett, M. C., Multiplexing Spheroid Volume, Resazurin and Acid Phosphatase Viability Assays for High-Throughput Screening of Tumour Spheroids and Stem Cell Neurospheres. *PLOS ONE* **2014**, *9* (8), e103817.
5. Torre, M. H.; Gambino, D.; Araujo, J.; Cerecetto, H.; Gonzalez, M.; Lavaggi, M. L.; Azqueta, A.; Lopez de Cerain, A.; Vega, A. M.; Abram, U.; Costa-Filho, A. J., Novel Cu(II) quinoxaline N1,N4-dioxide complexes as selective hypoxic cytotoxins. *European journal of medicinal chemistry* **2005**, *40* (5), 473-80.
6. Vieites, M.; Noblía, P.; Torre, M. H.; Cerecetto, H.; Laura Lavaggi, M.; Costa-Filho, A. J.; Azqueta, A.; de Cerain, A. L.; Monge, A.; Parajón-Costa, B.; González, M.; Gambino, D., Selective hypoxia-cytotoxins based on vanadyl complexes with 3-aminoquinoxaline-2-carbonitrile-N1,N4-dioxide derivatives. *Journal of inorganic biochemistry* **2006**, *100* (8), 1358-1367.
7. Lin, P.-S.; Ho, K.-C., New cytotoxic mechanism of the bioreductive agent Tirapazamine (SR 4233) mediated by forming complex with copper. *Radiation Oncology Investigations* **1996**, *4* (5), 211-220.
8. Tabassum, S.; Al-Asbahy, W. M.; Afzal, M.; Arjmand, F.; Bagchi, V., Molecular drug design, synthesis and structure elucidation of a new specific target peptide based metallo drug for cancer chemotherapy as topoisomerase I inhibitor. *Dalton Trans* **2012**, *41* (16), 4955-4964.
9. Leo, A.; Jow, P. Y. C.; Silipo, C.; Hansch, C., Calculation of hydrophobic constant (log P) from .pi. and f constants. *J Med Chem* **1975**, *18* (9), 865-868.
10. Eros, D.; Kovessi, I.; Orfi, L.; Takacs-Novak, K.; Gy, A.; Gy, K., Reliability of logP Predictions Based on Calculated Molecular Descriptors: A Critical Review. *Curr Med Chem* **2002**, *9* (20), 1819-1829.
11. Machatha, S. G.; Yalkowsky, S. H., Comparison of the octanol/water partition coefficients calculated by ClogP®, ACDlogP and KowWin® to experimentally determined values. *Int J Pharm* **2005**, *294* (1), 185-192.
12. Hay, M. P.; Gamage, S. A.; Kovacs, M. S.; Pruijn, F. B.; Anderson, R. F.; Patterson, A. V.; Wilson, W. R.; Brown, J. M.; Denny, W. A., Structure-activity relationships of 1,2,4-benzotriazine 1,4-dioxides as hypoxia-selective analogues of tirapazamine. *J Med Chem* **2003**, *46* (1), 169-82.
13. Valderrama-Negrón, A. C.; Alves, W. A.; Cruz, Á. S.; Rogero, S. O.; de Oliveira Silva, D., Synthesis, spectroscopic characterization and radiosensitizing properties of acetato-bridged copper(II) complexes with 5-nitroimidazole drugs. *Inorganica Chimica Acta* **2011**, *367* (1), 85-92.
14. Poole, J. S.; Hadad, C. M.; Platz, M. S.; Fredin, Z. P.; Pickard, L.; Guerrero, E. L.; Kessler, M.; Chowdhury, G.; Kotandeniya, D.; Gates, K. S., Photochemical electron transfer reactions of tirapazamine. *Photochemistry and photobiology* **2002**, *75* (4), 339-45.